Sixth International Symposium on Turbulence and Shear Flow Phenomena
Seoul, Korea, 22-24 June 2009

# GLOBAL STABILITY ANALYSIS OF COMPRESSIBLE LEADING-EDGE FLOW ON A SWEPT WING

**Christoph J. Mack**
Laboratoire d'Hydrodynamique (LadHyX),
CNRS-École Polytechnique
F-91128 Palaiseau cedex, France
cmack@ladhyx.polytechnique.fr

**Peter J. Schmid**
Laboratoire d'Hydrodynamique (LadHyX),
CNRS-École Polytechnique
F-91128 Palaiseau cedex, France
peter@ladhyx.polytechnique.fr

**Jörn L. Sesterhenn**
Department of Numerical Mathematics (LRT1),
Universität der Bundeswehr (UniBw) München
D-85577 Munich, Germany
jörn.sesterhenn@unibw.de

## ABSTRACT

The global hydrodynamic stability of compressible leading-edge flow on a swept wing is addressed using Krylov-based iterative methods in conjunction with direct numerical simulations (DNS). Such a global hydrodynamic stability solver enables the analysis of complex fluid behavior by extracting global stability information directly from numerical simulations. Applying the DNS-based stability approach, unstable boundary-layer modes of the crossflow type and amplified as well as weakly-damped acoustic modes have been computed for a supersonic flow configuration. A parameter study reveals that, depending on the spanwise disturbance wavenumber $\beta$, boundary-layer modes or acoustic modes represent the dominant instability mechanism for the investigated parameter choices. Furthermore, the results of the present work clearly demonstrate the necessity of a global stability analysis to comprehensively understand the stability of swept leading-edge flow.

## INTRODUCTION

Soon after the invention of aircraft in the beginning of the $20^{th}$ century it was realized that the aerodynamic design of high-performance aircraft crucially depends on a sound understanding of the compressible flow around wings. In particular, the details of the transition process from laminar to turbulent fluid motion, which causes increased drag and a loss of flight performance, play a dominant role in the description of this flow. Two-dimensional hydrodynamic instabilities of the Tollmien–Schlichting type have been found to trigger this transition process and to cause transition in the downstream direction for unswept wings (see figure 1, TS region).

With the invention of high-speed aircraft in the 1940s, the introduction of sweep became necessary to overcome serious design problems emanating from compressibility effects such as the shock stall phenomenon. The first theoretical and experimental investigations on swept wings suggested that the presence of sweep does not affect the stability of the flow. However, in later flight tests on swept wing aircraft, Gray (1952) found that beyond a critical speed $q_\infty$, the transition front moved toward the attachment line of the wing; this phenomenon could not be explained by existing two-dimensional arguments. He further observed this critical speed to be a function of the sweep angle $\Lambda$ as well as the leading-edge radius $R$ of the wing (see figure 1).

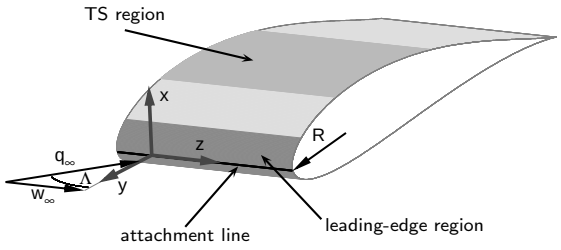


Figure 1: Sketch of a swept wing showing the attachment line, the leading-edge region, the incoming velocity $q_\infty$ and the sweep angle $\Lambda$ yielding a sweep velocity $w_\infty$, as well as the local Cartesian coordinate system.

The theoretical and experimental investigations that followed revealed a new type of instability, the crossflow instability, which is due to a crossflow velocity inside the boundary layer. The presence of sweep (and curvature) lead to a highly three-dimensional boundary-layer flow in the leading-edge region of a swept wing and, thus, fundamentally render its inherent stability properties; the initially two-dimensional boundary-layer flow gradually merges into a three-dimensional flow downstream of the attachment line (see, e.g., Bippes, 1999; Saric et al., 2003, for a detailed description of this flow).

However, subsequent experiments revealed once more a lack of understanding of swept leading-edge flow, since their results on leading-edge transition could not be explained by destabilized crossflow vortices alone. Conducting wind-tunnel experiments on a swept wing, Poll (1978) concluded that the flow configuration is also susceptible to instabilities right at the attachment line. In the following, two instability mechanisms, the amplification of perturbations in the swept attachment-line boundary layer, known as *attachment-line* instabilities, and the amplification of crossflow vortices in the three-dimensional boundary layer further downstream, denoted as *crossflow* instabilities, have been suggested to trigger transition (see Saric et al., 2003; Le Duc et al., 2006, and the references therein for an overview of the relevant literature).

#### Global stability investigations

In the past, these two instability mechanisms have been studied *separately* (see Mack et al., 2008a, for an overview), despite a general acknowledgment that they coexist under realistic conditions as indicated by Bertolotti (1999). The subdivision of the flow configuration into different parts and the resulting separate treatment of these two instability mechanisms has been the consequence of a necessary simplification of the complex flow problem in order to treat it with classical tools of hydrodynamic stability theory. The recent progress in computational fluid dynamics (both in terms of hardware and software) and in global stability analysis, however, permitted Mack and Schmid (2009) to develop a numerical tool to address the global stability of large-scale flow problems and, thus, to study a more realistic configuration that covers *simultaneously* attachment-line and crossflow vortex instabilities (Mack et al., 2008a). As a result, boundary-layer modes that establish a connection between attachment-line and crossflow modes could be computed which further display the least-stable structures for the investigated parameter settings. This result clearly demonstrates the necessity of a global stability analysis in order to comprehensively understand the stability of swept leading-edge flow.

The contribution of this article can be seen as an extension of the latter work (Mack et al., 2008a) towards a different parameter choice as well as a discussion on the influence of compressibility onto the global spectrum. Considering the influence of compressibility has the following two reasons: (i) it is known that compressibility effects influence the stability properties of the above-described instability mechanisms (Lin and Malik, 1995; Le Duc et al., 2006) and (ii) supersonic and hypersonic boundary-layer flows have been found to additionally feature acoustic instabilities, known as *Mack modes* (Mack, 1984). Increasing the governing Mach number, the latter modes become more and more unstable, but up to moderate Mach regimes, they are less amplified than boundary-layer modes; for high Mach number flows, however, the Mack modes display the dominant instability for boundary-layer flows as reported by Mack (1984). Consequently, the prevailing instability mechanism for compressible leading-edge flow on a swept wing is determined by the particular flow configuration featuring a highly three-dimensional boundary-layer flow about a complex geometry as well as compressibility.

#### Flow configuration & direct numerical simulations

In what follows, we focus on the global stability of compressible flow in the leading-edge region of a swept wing

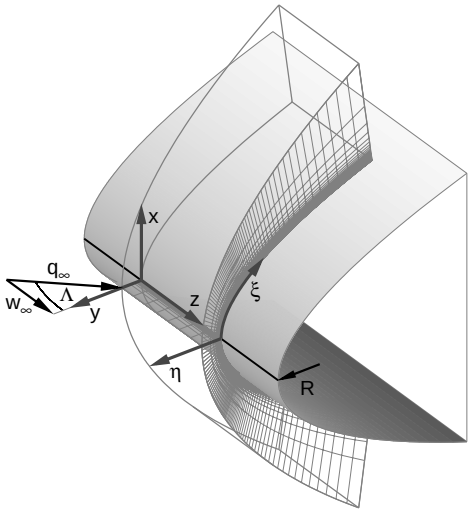


Figure 2: Sketch of our three-dimensional flow model displaying the relevant flow parameters, the coordinate systems and the body-fitted grid with its grid-point distribution.

where the incoming flow impinges onto the body with a velocity $q_\infty$ and a sweep angle $\Lambda$ yielding a sweep velocity $w_\infty$ and a wall-normal velocity $v_\infty$ (see figure 1). This flow configuration is modeled by flow about a swept parabolic body of infinite span with the leading-edge radius $R$ as shown in figure 2, where the flow impinges through a detached bow shock onto the body forming a local stagnation flow near the attachment line which further downstream turns into a three-dimensional curved boundary-layer flow.

We define a viscous length scale $\delta$, a sweep Reynolds number $Re_s$ and a sweep Mach number $Ma_s$ as

$$\delta = \left(\frac{\nu_r}{S}\right)^{1/2}, \quad Re_s = \frac{w_\infty \delta}{\nu_r}, \quad Ma_s = \frac{w_\infty}{c_\infty}$$

respectively, where $\nu_r$ denotes the kinematic viscosity, $S$ is the strain rate at the wall and $c_\infty$ is the speed of sound. Alternatively, the sweep Reynolds number $Re_s$ can be reformulated to display an explicit dependence on the leading-edge radius $R$ and the sweep angle $\Lambda$.

$$Re_s = \left(\frac{v_\infty R}{2\nu_r}\right)^{1/2} \tan\Lambda \tag{1}$$

The three-dimensional boundary-layer flow is computed via direct numerical simulations (DNS), where the compressible Navier–Stokes equations (2a–c), which are formulated based on pressure $p$, velocities $(u, v, w)$ and entropy $s$ using Cartesian tensor notation, govern the flow.

$$\frac{\partial p}{\partial t} + u_j \frac{\partial p}{\partial x_j} + \gamma p \frac{\partial u_j}{\partial x_j} = \frac{p}{C_v}\left(\frac{\partial s}{\partial t} + u_j \frac{\partial s}{\partial x_j}\right) \tag{2a}$$

$$\frac{\partial u_i}{\partial t} + u_j \frac{\partial u_i}{\partial x_j} + \frac{1}{\varrho}\frac{\partial p}{\partial x_i} = \frac{1}{\varrho}\tau_{ij} \tag{2b}$$

$$\frac{\partial s}{\partial t} + u_j \frac{\partial s}{\partial x_j} = \frac{R}{p}\left(\Phi + \frac{\partial}{\partial x_j}\left(k\frac{\partial T}{\partial x_j}\right)\right) \tag{2c}$$

with

$$\Phi \equiv \frac{1}{2}\mu\left(\frac{\partial u_i}{\partial x_j} + \frac{\partial u_j}{\partial x_i}\right)^2 - \frac{2}{3}\mu\left(\frac{\partial u_k}{\partial x_k}\right)^2$$

$$\tau_{ij} \equiv \frac{\partial}{\partial x_j}\left(\mu\left(\frac{\partial u_i}{\partial x_j} + \frac{\partial u_j}{\partial x_i}\right) - \frac{2}{3}\mu\frac{\partial u_k}{\partial x_k}\delta_{ij}\right)$$

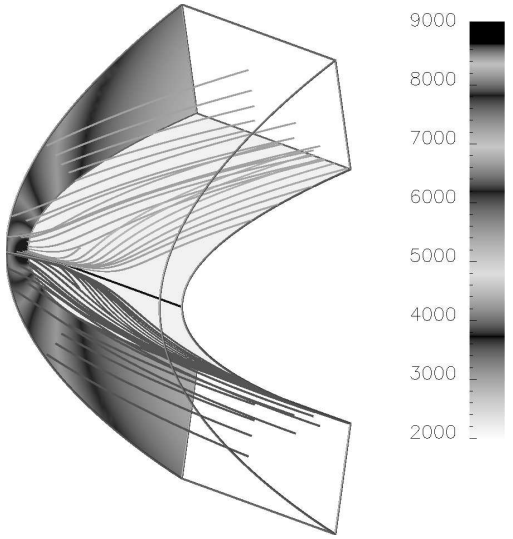


Figure 3: Pressure field [in Pa] and streamlines of the computed steady base flow for $Re_s = {}^{w_\infty\delta}/_{\nu} = 800$ and $Ma_s = {}^{w_\infty}/_{c_\infty} = 1.25$. The resolution is $128 \times 255$ points in the normal $\eta$-direction and the chordwise $\xi$-direction, respectively (attachment line in black); a leading-edge radius of $R = 0.1 = 508\delta$ [in m] has been used.

Herein, the variables $\varrho$, $T$, $\mu$ and $k$ denote, respectively, the density, the temperature, the dynamic viscosity and the thermal conductivity, and $C_v$ is the specific heat at constant volume, $R$ the gas constant and $\delta_{ij}$ the Kronecker delta. We consider the motion of a compressible fluid modeled as a perfect gas with constant specific heat ratio $\gamma = 1.4$ and constant Prandtl number $Pr = 0.71$. The equation of state, Fourier's law for the thermal conductivity and Sutherland's law (at ambient conditions) for the viscosity further describe the flow. The equations (2a–c) are solved on a time-dependent, curvilinear and non-uniformly distributed grid, with a clustering of the grid points in the relevant regions. The governing equations are discretized employing fifth- and sixth-order compact schemes (see Sesterhenn, 2001; Mack et al., 2008a, and the references therein for details on the implementation of the direct numerical simulations).

In the past, direct numerical simulations (DNS) have been successfully applied to locally investigate swept leading-edge flow using planar geometries. These simulations employed distinct flow models for flow in the vicinity of the attachment line and for flow further downstream to address attachment-line and crossflow instabilities, respectively. As an example, Spalart (1988) and Joslin (1995) studied incompressible attachment-line flow, Le Duc et al. (2006) addressed the compressible case, and Bonfigli and Kloker (2007) investigated the stability of crossflow vortices. Recently however, Mack et al. (2008a) performed a *global* stability analysis of compressible leading-edge flow based on direct numerical simulations (see introduction).

## GLOBAL STABILITY ANALYSIS

In a first step towards a global stability analysis the governing equations (2a–c) are integrated in time by a fourth-order Runge–Kutta method to obtain a steady base flow $\phi_0(x, y) = (p_0, u_0, v_0, w_0, s_0)^T$. This base flow is displayed in figure 3 in terms of pressure field and streamlines which are highly curved, in particular, close to the attachment line.

The governing equations are then linearized by superimposing a three-dimensional disturbance field $\phi'(x, y, z, t)$ onto the steady base flow, and for the global stability approach $\phi'(x, y, z, t)$ is assumed to satisfy the following traveling-wave form.

$$\phi'(x, y, z, t) = \widetilde{\phi}(x, y)\mathrm{e}^{\mathrm{i}(\beta z - \omega t)} \tag{3}$$

Herein, $\widetilde{\phi}(x, y)$ denotes the complex amplitude and $\beta$ the real spanwise wavenumber of the perturbation. The latter parameter results from a Fourier decomposition in the spanwise $z$-direction as part of this assumption. The long-term temporal stability of the perturbation is given by the global eigenvalue $\omega$ whose real part describes the frequency $\omega_r$ and whose imaginary part the corresponding growth rate $\omega_i$.

Under assumption (3) and an appropriate discretization of the $\xi$- and $\eta$-dependence, a global stability analysis of the flow configuration displayed in figure 2 finally requires us to solve a large-scale eigenvalue problem

$$\lambda\mathbf{x} = \mathbf{A}\mathbf{x} \tag{4}$$

where $\mathbf{x} \equiv \widetilde{\boldsymbol{\phi}}(x, y)$ and $\lambda \equiv \omega$, and $\mathbf{A} \equiv \boldsymbol{J}(\boldsymbol{\phi}_0)$ represents the $n \times n$ linear stability matrix (the Jacobian), i.e., the discrete compressible Navier–Stokes equations linearized about the base state $\boldsymbol{\phi}_0$, with $n = 5n_\xi n_\eta$ as the dimension of this eigenvalue problem; $n_\xi$ and $n_\eta$ denote the number of grid points in the $\xi$- and $\eta$-direction, respectively. For large $n$, the direct solution of (4) is prohibitively expensive, and iterative solution techniques have to be employed to extract pertinent stability information.

### Iterative solution technique

The algorithm to accomplish this task is the implicitly restarted Arnoldi method (IRAM), a Krylov subspace technique presented by Sorensen (2002). This method constructs an orthonormal basis

$$\mathbf{V}_m = [\mathbf{v}_1, \mathbf{v}_2, \ldots, \mathbf{v}_m] \tag{5}$$

of the Krylov subspace $\mathcal{K}_m(\mathbf{v}_1, \mathbf{A})$, starting with an initial vector $\mathbf{v}_1$, which is then used to decompose the stability matrix $\mathbf{A}$ in the following way.

$$\mathbf{A}\mathbf{V}_m = \mathbf{V}_m\mathbf{H}_m + \mathbf{f}_m\mathbf{e}_m^T \tag{6}$$

Herein, $\mathbf{H}_m$ denotes an $m$-dimensional upper Hessenberg matrix (with $m \ll n$), $\mathbf{f}_m$ is the residual vector orthogonal to the basis $\mathbf{V}_m$, and $\mathbf{e}_m$ represents a unit-vector in the $m$-th component.

The eigenvalues $\{\theta_j\}$ of the Hessenberg matrix $\mathbf{H}_m$, the so-called Ritz values, represent approximations of the eigenvalues $\{\lambda_j\}$ of the matrix $\mathbf{A}$, and the associated eigenvectors $\widetilde{\mathbf{x}}_j$ of $\mathbf{A}$, the so-called Ritz vectors, can be calculated using the orthonormal basis $\mathbf{V}_m$ as $\widetilde{\mathbf{x}}_j = \mathbf{V}_m\mathbf{y}_j$, where $\mathbf{y}_j$ denotes the eigenvector of $\mathbf{H}_m$ associated with the eigenvalue $\theta_j$. In general, some of the Ritz pairs ($\widetilde{\mathbf{x}}_j$,$\theta_j$) closely approximate some eigenpairs ($\mathbf{x}_j$,$\lambda_j$) of $\mathbf{A}$, and the quality of this approximation usually improves as the dimension $m$ of the Krylov subspace sequence $\mathcal{K}_m$ increases. In order to avoid memory problems and numerical errors as $m$ increases, the Arnoldi method is implicitly restarted from the $k$ desired Ritz pairs (see Sorensen, 2002).

When applied in a straightforward manner, the implicitly restarted Arnoldi method generally computes the least stable part, represented by some of the least stable modes, of the full global spectrum; these modes typically display

the desired stability information. On the other hand, flow configurations as complicated as ours feature a multitude of physical processes — boundary-layer modes, acoustic modes, etc. — which will also be reflected in the global spectrum. Furthermore, the different types of modes exhibit variable growth rates $\omega_i$ and additionally travel with a distinct frequency $\omega_r$. As a consequence, the Arnoldi method cannot straightforwardly be used to access selected modes of the global spectrum, which prevents a comprehensive global stability investigation (see Mack and Schmid, 2009).

#### Cayley transformation

To overcome the latter limitation and to increase the flexibility of the Arnoldi method, a spectral transformation is added. This transformation is given by the Cayley transformation, which consists of a two-parameter conformal mapping of the complex plane; the first mapping parameter, $\sigma$, acts as a shift parameter about which the spectrum is inverted, and the second mapping parameter, $\mu$, is mainly used to control the condition number of the mapped system.

This transformation requires, however, the solution of the following generally non-Hermitian linear system

$$(\mathbf{A} - \sigma\mathbf{I})\mathbf{v}_{i+1} = (\mathbf{A} - \mu\mathbf{I})\mathbf{v}_i \tag{7}$$

where $\mathbf{I}$ denotes the identity matrix, for each outer step of the Arnoldi method to construct the $(i+1)$-th basis vector in (5). This is accomplished by using the Krylov-based iterative linear solver BiCGStab (van der Vorst, 1992). The application of an iterative system solver, however, limits the choice of the Cayley parameters, and the shift $\sigma$ has to be chosen sufficiently far away from an eigenvalue to allow the system solver to converge.

An efficient iterative solution of the linear system (7) requires a reliable and robust preconditioning technique. To accomplish this, we linearize the compressible Navier–Stokes equations and explicitly compute a Jacobian matrix $\mathbf{P}$ based on a low-order spatial discretization, e.g, using a second-order finite-difference scheme. The sparsity of $\mathbf{P}$ enables us to apply sparse techniques to store and efficiently invert it. The latter task is accomplished by employing incomplete decomposition techniques (see Saad, 2003).

#### DNS-based implementation

The Arnoldi method as well as BiCGStab belongs to the class of Krylov subspace methods which benefits from the fact that they only require the action of the Jacobian matrix $\mathbf{A} \equiv \boldsymbol{J}(\boldsymbol{\phi}_0)$ onto a given flow field $\mathbf{v} \equiv \boldsymbol{\phi}'(x, y)$. These matrix-vector products can readily be obtained from direct numerical simulations via

$$\mathbf{A}\mathbf{v} \approx \frac{\mathbf{F}(\boldsymbol{\phi}_0 + \epsilon\mathbf{v}) - \mathbf{F}(\boldsymbol{\phi}_0)}{\epsilon} \tag{8}$$

where $\epsilon$ is a user-specified parameter, chosen as $||\epsilon\mathbf{v}||/||\boldsymbol{\phi}_0|| = \epsilon_0 = 10^{-8}$, and $\mathbf{F}$ represents the discretized right-hand side of the nonlinear Navier–Stokes equations. This first-order finite-difference approximation of the Jacobian matrix $\boldsymbol{J}(\boldsymbol{\phi}_0)$ allows a Jacobian-free framework where right-hand side evaluations from direct numerical simulations (DNS) provide the input for the iterative stability solver; it has to be mentioned that this input could come from any numerical simulations (large eddy simulations (LES), detached eddy simulations (DES), etc.). For a detailed description of the DNS-based global stability solver we refer the reader to Mack and Schmid (2009).

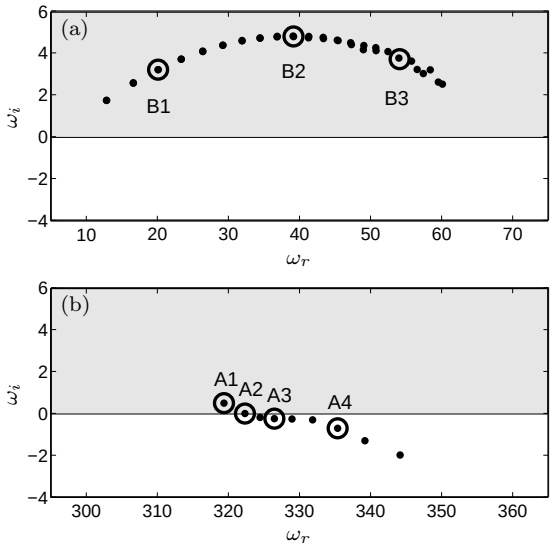


Figure 4: Computed subsets of the full global spectrum for $\beta = 0.224$ ($\omega_r$ describes the frequency and $\omega_i$ the corresponding growth rate of the perturbation; unstable half-plane in grey): (a) eigenvalues belonging to boundary-layer modes of the crossflow type and (b) eigenvalues belonging to acoustic modes.

## RESULTS

The DNS-based iterative scheme was employed to investigate the global stability of a compressible flow about the parabolic body as depicted in figure 2. The flow parameters were $Re_s = 800$, $Ma_s = 1.25$ and $T_w = 728K$ (adiabatic wall), the resolution was $128 \times 255$ points in the wall-normal $\eta$- and the chordwise $\xi$-direction, respectively, and the disturbance wavenumber was $\beta = 2\pi/L_z = 0.224$. Furthermore, localized white noise was used as initial condition in (5). In their work, Mack et al. (2008a) present global boundary-layer modes for a smaller disturbance wavelength $L_z$ using $\beta = 0.314$, and they further found the present parameter choice to be highly unstable to three-dimensional perturbations (see Mack et al., 2008b, for a discussion on the influence of $Re_s$ on the global stability of boundary-layer modes).

#### Global spectrum

As results, two computed subsets of the full global spectrum are shown in figure 4. The eigenvalues displayed in (a) correspond to boundary-layer modes of the crossflow type and reveal the least-stable part, a three-dimensionally unstable discrete branch, of the global spectrum. Furthermore, these modes feature a rather low frequency $12.9 \lesssim \omega_r \lesssim 62.6$ for disturbances traveling in the spanwise $z$-direction; the maximum growth rate $\omega_i = 4.85$ is achieved for a frequency $\omega_r = 39.1$. In figure 4(b) we present eigenvalues which correspond to amplified ($\omega_i = 0.516$) and weakly-damped acoustic global modes. In contrast to the boundary-layer modes, these modes are fast traveling $319 \lesssim \omega_r \lesssim 344$ and more stable; the high frequency $\omega_r$ reflects the supersonic character of the flow in the spanwise $z$-direction. Both subsets have been obtained by performing computations with a selected choice of the complex-valued parameters $\sigma$ and $\mu$ ($\mu_r = \sigma_r$, $\mu_i/\sigma_i = 4$): $\sigma = 16 + 270\mathrm{i}$ and $57 + 270\mathrm{i}$ to compute the subset in (a) and $\sigma = 330 + 160\mathrm{i}$ to find the subset in (b).

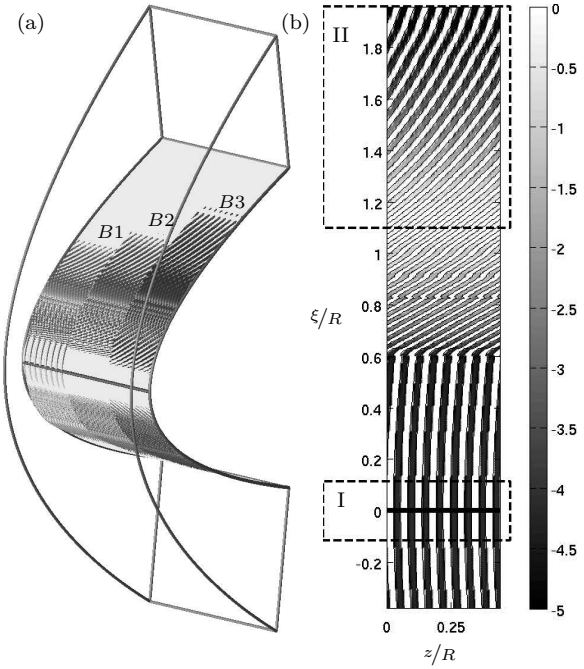


Figure 5: (a) Three associated global modes displaying the velocity distribution $v(x,y,z) = \mathrm{Real}\{\widetilde{v}(x,y)\,(\cos\beta z + \mathrm{i}\sin\beta z)\}$ of three eigenvalues depicted by circles in figure 4(a); the normalized eigenfunctions are plotted using iso-surfaces with a value of $10^{-5}\ v_{max}$, and eight wavelengths, stretched by a factor of two, in the spanwise $z$-direction. (b) Top view of mode B1 in the $\xi z$-plane at approximately half the boundary-layer thickness $\delta_{99}$ ($\delta_{99} \approx 2.38\delta$ at the attachment line); a log-scale was used to visualize the positive values of $v$; iso-contour lines of zero amplitude in black.

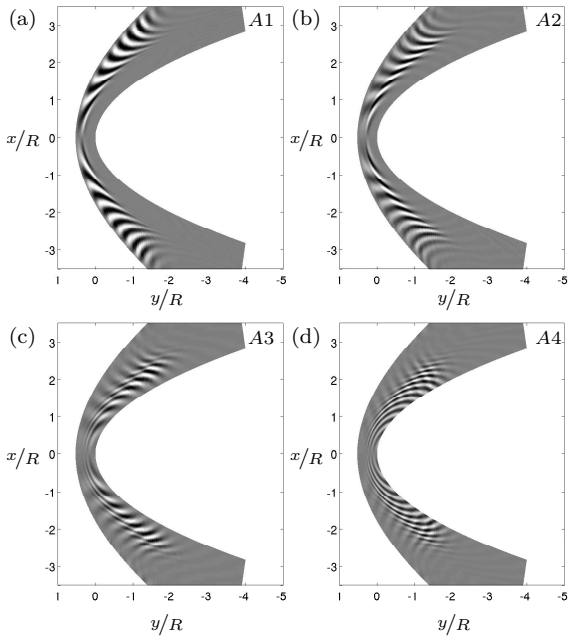


Figure 6: Spatial structure of a sample of associated global acoustic modes visualized by the chordwise velocity $u(x,y,z)$ in the $xy$-plane: (a) unstable mode A1 and (b,c,d) faster-traveling stable modes (A2,A3,A4), respectively, from the acoustic branch displayed in figure 4(b); large amplitudes in black.

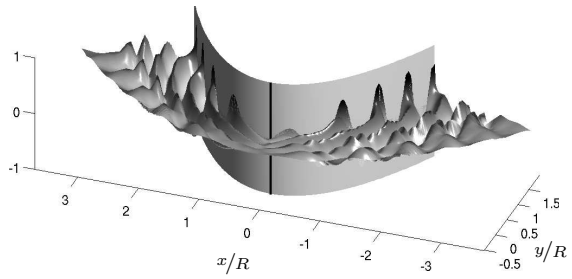


Figure 7: Spatial shape of the velocity component $u(x,y,z)$ of the acoustic mode A4 (see figure 6d) in the $xy$-plane.

#### Boundary-layer instabilities

The spatial distribution of three associated eigenfunctions $v(x,y,z) = \mathrm{Real}\{\widetilde{v}(x,y)\,(\cos\beta z + \mathrm{i}\sin\beta z)\}$ belonging to the boundary-layer instabilities shown in figure 4(a) are presented in figure 5(a). A slow moving global mode (B1) reveals a connection between attachment-line instabilities and crossflow vortices as reported in Mack et al. (2008a), and faster moving global modes (B2,B3) show a more pronounced crossflow component, and the dominant part of the global mode lies further downstream from the attachment line. The connection mode (B1) exhibits a two-dimensional structure near the attachment-line consisting of chordwise vortices with a specific spanwise scale $L_z$. It gradually merges into a three-dimensional mode further downstream and eventually forms vortical structures which nearly align with the external streamlines (see figure 5b). These vortical structures result from co-rotating vortices and display the familiar crossflow pattern.

The two-dimensional character of this mode in the vicinity of the attachment line (see figure 5b, range I) is reminiscent of attachment-line instabilities, and the spatial structure of such instabilities can be found in Joslin (1995). Furthermore, co-rotating vortices (see figure 5b, range II) are typical for the crossflow instability, and flow visualizations of such vortices are shown in Bonfigli and Kloker (2007). Moreover, streaky structures produced by crossflow vortices were seen in Gray's (1952) flight tests as well as in Poll's (1978) wind-tunnel experiments on swept wings.

#### Acoustic instabilities

In the presence of compressibility, the global spectrum additionally features fast propagating acoustic modes (see figure 4b) that describe the presence of sound waves. The structure of such modes is presented in figure 6, where the amplitude distribution of the chordwise velocity $u(x,y,z)$ of amplified and weakly-damped acoustic global modes is shown. The unstable (A1) as well as the least stable mode (A2) show a dominant spatial structure downstream of the detached bow shock which disappears close the surface of the body; the bow shock can be interpreted as a "wall" which prevents sound waves to travel upstream of the shock.

More stable modes (A3,A4) exhibit smaller spatial structures which eventually extend into the boundary layer (see figure 7). Furthermore, the acoustic modes reveal a two-dimensional shape in the vicinity of the attachment line.

#### Parameter studies

As detailed above, compressible flow in the leading-edge region of a swept wing is governed by a large number of physical and geometric parameters. Mack et al. (2009) chose to

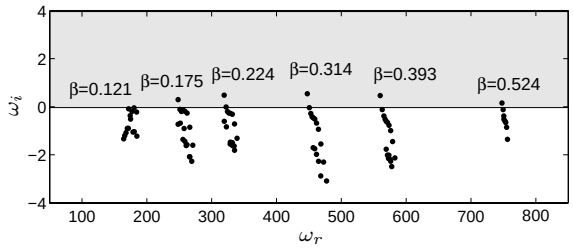


Figure 8: Computed temporal spectra belonging to acoustic global modes for selected spanwise wavenumbers $\beta$.

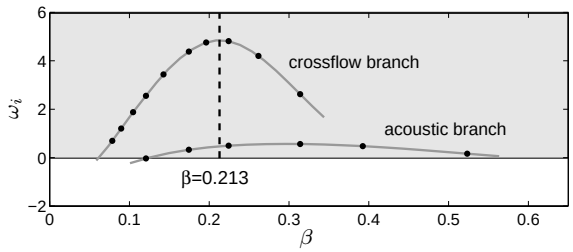


Figure 9: Temporal growth rate $\omega_i$ as a function of the disturbance wavenumber $\beta$.

present a parametric study of the stability of boundary-layer modes of the crossflow type with respect to the spanwise wavenumber $\beta$. Results from a similar study are shown in figure 8, where the influence of $\beta$ on the stability of acoustic global modes is considered for spanwise wavenumbers ranging from 0.121 to 0.524. For this parameter choice, each configuration displays one unstable acoustic mode.

As did the boundary-layer modes, the acoustic modes reveal a similar spanwise dependence, a steadily growing growth rate $\omega_i$ before decaying again (see figure 9). Furthermore, the acoustic branch appears to grow up to $\beta \approx 0.314$, while Mack et al. (2009) report a maximum modal growth of boundary-layer modes for $\beta = 0.213$ (crossflow branch). The results in figure 9 further indicate, that the acoustic modes become the dominant instability for rather large wavenumbers $\beta > 0.380$ for the investigated base flow.

## CONCLUSIONS

A DNS-based global stability solver was successfully applied to assess the global spectrum of compressible flow in the leading-edge region of a swept wing modeled by a parabolic body. Using this solver, unstable boundary-layer modes of the crossflow type and amplified as well as weakly-damped acoustic modes have been computed for a supersonic flow configuration. It was found that, depending on the spanwise wavenumber $\beta$, boundary-layer modes or acoustic modes represent the dominant instability mechanism for the investigated parameter choices. In summary, it was shown that the employed DNS-based Krylov technique allows the conversion of modern numerical simulations into diagnostic tools for hydrodynamic global stability analysis of large-scale complex flows.

## KNOWLEDGEMENTS

Financial support from the Deutsche Forschungsgemeinschaft (DFG), the Studienstiftung des Deutschen Volkes, the Alexander-von-Humboldt Foundation and the ANR program “Chaires d’excellence” is gratefully acknowledged. This first author also wants to warmly thank Rainer Friedrich for his support during the start of his PhD studies.

## REFERENCES

Bertolotti, F. P., 1999, “On the connection between cross-flow vortices and attachment-line instabilities”, *IUTAM Symp. on Laminar-Turbulent Transition*, Sedona, USA, pp. 625-630.

Bippes, H., 1999, “Basic experiments on transition in three-dimensional boundary layers dominated by crossflow instability”, *Prog. Aero. Sci.*, Vol. 35, pp. 363-412.

Bonfigli, G., Kloker, M., 2007, “Secondary instability of crossflow vortices: validation of the stability theory by direct numerical simulation”, *J. Fluid Mech.*, Vol. 583, pp. 229-272.

Gray, W. E., 1952, “The effect of wing sweep on laminar flow”, *British Royal Aircraft Establishment*, RAE TM Aero 255.

Joslin, R. D., 1995, “Direct simulation of evolution and control of three-dimensional instabilities in attachment-line boundary layers”, *J. Fluid Mech.*, Vol. 291, pp. 369-392.

Le Duc, A., Sesterhenn, J., and Friedrich, R., 2006, “Instabilities in compressible attachment-line boundary layers”, *Phys. Fluids*, Vol. 18, 044102.

Lin, R. S., Malik, M. R., 1995, “Stability and transition in compressible attachment-line boundary-layer flow”, *SAE*, 952041.

Mack, L. M., 1984, “Boundary Layer Linear Stability Theory”, Special Course on Stability and Transition of Laminar Flow, *AGARD–R–709*.

Mack, C. J., Schmid, P. J., and Sesterhenn, J. L., 2008a, “Global stability of swept flow around a parabolic body: connecting attachment-line and crossflow modes”, *J. Fluid Mech.*, Vol. 611, pp. 205-214.

Mack, C. J., Schmid, P. J., and Sesterhenn, J. L., 2008b, “Global stability analysis of compressible flow around swept wings”, *In: Notes Num. Fluid Mech.*, Springer, accepted.

Mack, C. J., and Schmid, P. J., 2009, “A preconditioned Krylov technique for global hydrodynamic stability analysis of large-scale compressible flows”, *J. Comput. Phys.*, submitted.

Poll, D. I. A., 1978, “Some aspects of the flow near a swept attachment line with particular reference to boundary layer transition”, *Cranfield Institute of Technology*, CoA 7805.

“Transition in the infinite swept attachment-line boundary layer”, *Aero. Q.*, Vol. 30, pp. 607-628.

Saad, Y., 2003, “Iterative Methods for Sparse Linear Systems, Second Edition”, *Society for Industrial and Applied Mathematics*.

Saric, W. S., Reed, H. L., and White, E. B., 2003, “Stability and transition of three-dimensional boundary layers”, *Annu. Rev. Fluid Mech.*, Vol. 35, pp. 413-440.

Sesterhenn, J., 2001, “A characteristic-type formulation of the Navier–Stokes equations for high-order upwind schemes”, *Comput. Fluids*, Vol. 30, pp. 37-67.

Sorensen, D. C., 2002, “Numerical methods for large eigenvalue problems”, *Acta Numer.*, Vol. 11, pp. 519-584.

Spalart, P. R., 1988, “Direct numerical study of leading-edge contamination”, *AGARD-CP-438*, 5/1–5/13.

van der Vorst, H. A., 1992, “Bi-CGSTAB: A fast and smoothly converging variatn of Bi-CG for the solution of non-symmetric linear systems”, *SIAM J. Sci. Statist. Comput.*, Vol. 13, pp. 631-644.